Available online at www.sciencedirect.com

SciVerse ScienceDirect

Procedia Engineering 59 (2013) 16 – 24

Procedia Engineering

www.elsevier.com/locate/procedia

3rd International Conference on Tissue Engineering, ICTE2013

Finite element analysis of axonal microtubule bundle under tension and torsion

Amirshahin Shahinnejad*, Mohammad Haghpanahi, Farhad Farmanzad

Iran University of Science and Technology, Narmak, Tehran 1684613114, Iran

Abstract

Microtubule bundles cross-linked by tau proteins are essential in many functions of neurological tissues, axons for instance, and play a fundamental role in keeping their mechanical integrity, facilitating their growth, and help promoting cargo transport. Damages resulted from Traumatic Brain Injuries (TBIs), lead to disorientation of these bundles and impose some cognitive damages to the patient as well as shortening the operability of axons themselves. This study shows that axonal microtubule bundle cross-linked by tau proteins under a uniaxial tension and torsion, which is, to our knowledge, the first 3D finite element model to investigate mechanical properties of axonal microtubule bundle. The results show strain-stiffening behavior of these bundles under uniaxial tension. We also investigated the behavior of each bundle under torsional loading and derived modulus of rigidity for each cross-link spacing bundle which may shed light on making neurological scaffolds as we may have more realistic model and will be able to select materials with mechanical properties with better agreement with that of the real tissue.

Selection and peer-review under responsibility of the Centre for Rapid and Sustainable Product Development, Polytechnic Institute of Leiria, Centro Empresarial da Marinha Grande.

Keywords: Finite Element Analysis; Axon; Microtubule Bundle; Tau Protein; Tension; Torsion; Modulus of Rigidity.

* Corresponding author. Tel.: +98-912-714-5265; fax: +98-21-8808-2296.
E-mail address: a_shahinnejad@mecheng.iust.ac.ir

Selection and peer-review under responsibility of the Centre for Rapid and Sustainable Product Development, Polytechnic Institute of Leiria, Centro Empresarial da Marinha Grande
doi:10.1016/j.proeng.2013.05.088

1. Introduction

Microtubule bundles cross-linked by microtubule-associated protein (MAP) tau are a major structural feature of the axon, an elongated projection that conducts electrical impulses away from the body of a neuron. These microtubule bundles are located in the interior portion of the axon, and alongside neurofilaments and a thin actin cortex form the axonal cytoskeleton. A variety of neurological functions are mediated by these bundles, including maintaining mechanical integrity and shape of the axon, promoting axonal growth, and facilitating cargo transport [1, 2]. Axonal microtubule bundles typically contain a density of microtubules of ~10–200 microtubules/mm^2, yielding ~10–100 microtubules in a typical cross section [3]. It has been found that the average length of these microtubules is ~4 μm in the axon of cultured rat hippocampal neurons [4].

Traumatic axonal injury is a characteristic feature of focal and diffuse traumatic brain injury, characterized by local disorientation of the axonal microtubule bundle, beading of the axon, impaired axonal transport, retraction of the synapse, and axonal degeneration [5-8].

When the head is accelerated and decelerated abruptly in space, particularly when accompanied by a torsional head movement, strain forces are applied to nerve fibers (axons) throughout the brain [9, 10]. The resulting axonal strain injuries, collectively referred to as diffuse axonal injury (DAI), represent the primary fundamental neuropathological change seen in TBI due to closed mechanisms regardless of injury severity, although the amount of DAI increases as injury severity increases [11].

Strictly speaking, if the head moves abruptly enough, as in whiplash injuries, it need not strike or be struck by another object for acceleration-deceleration phenomena sufficient to cause an axonal strain injury within the brain to occur [9], and clinicians who work with TBI are familiar with cases, usually mild, in which no head impact is involved.

Computational modeling techniques have been employed to investigate the mechanical behavior of the filaments comprising the cytoskeleton [12, 13], and have been used to investigate axonal microtubule bundle under tension [14]. This study proposed a 3D finite element model to investigate mechanical behavior of axonal microtubule bundle under tension. We then apply torsional loading on the model to derive the modulus of rigidity for each bundle which has not been possible using current experimental techniques. The result of this study may shed light on making neurological scaffolds as we may have more realistic model and will be able to select materials with mechanical properties with better agreement with that of the real tissue.

2. Materials and Methods

2.1. Finite Element Analysis

Although a most exciting field of activity, engineering analysis is clearly only a support activity in the larger field of engineering design. The analysis process helps to identify good new designs and can be used to improve a design with respect to performance and cost. In the early use of finite element methods, only specific structures were analyzed, mainly in the aerospace and civil engineering industries. However, once the full potential of finite element methods was realized and the use of computers increased in engineering design environments, emphasis in research and development was placed upon making the use of finite element methods an integral part of the design process in mechanical, civil, and aeronautical engineering [15].

Today, the use of finite element analysis is not limited to any particular field of study and by development of powerful software, e.g. ABAQUS/CAE, CATIA, NASTRAN, and advanced computers, more extensive areas of science can be investigated to shed light on the unknown characteristics of the most unreachable sizes and geometries.

Here we used ABAQUS/CAE 6.10, [16], to develop our 3D finite element proposed model and analyzed it under steady state condition. We used the ABAQUS/CAE with standard/explicit model and built a 3D structure using beam elements.

2.2. Bundle Geometry

Using ABAQUS/CAE, a hexagonal bundle of 19 rows with a center-to-center microtubule spacing of 45 nm was created. Each row consisted of 8μm of microtubule length with one discontinuity; this created 38 separate microtubules with an average continuous microtubule length of 4μm. Discontinuities limited to be in the 80% central of each bundle and an arbitrary gap length of 150 nm was used at the discontinuity in each row. A representative bundle generated considering these constraints is shown in figure 1.

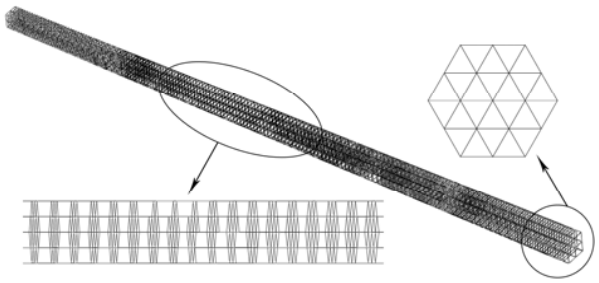

Figure 1. Example of geometry created using ABAQUS/CAE. Microtubules are placed with 45nm center-to-center spacing in 8μm rows with one arbitrary discontinuity and cross-links distributed with evenly spacing throughout the bundle. (50nm cross-link spacing bundle is shown)

4 different bundles created with different cross-link spacing of 25, 50, 75, and 100nm. Cross-links evenly distributed between microtubules according to each spacing. For each of the above spacing 5 different bundles created by randomizing the location of discontinuities in each row. These five configurations allowed for statistical significance and prevented skewing the results toward a particular configuration's response.

We assumed that microtubules are hollow cylinders with the outer diameter of 25nm and the inner diameter of 14nm [17].

2.3. Material Properties

The material properties used in this modeling were adapted from the work of Peter and Mofrad, 2012, and some corrections were made in order to simulate the behavior of microtubule-cross linking tau proteins system under uniaxial loading and obtain its response. The young modulus of cross linking tau proteins was assumed to be 5MPa [14]. In order to reduce the flexural behavior of these proteins, using Eq. 1, we elevated this constant to be 62.5MPa to have the same axial spring constant as that of Peter et al. These data are provided in Table 1.

Table 1. Material Properties of Microtubule and Cross-linking Tau Proteins used in the Simulations.

	Value	Reference
Microtubule Young's Modulus (N/nm2)	1.50E-08	[14]
Tau Proteins Young's Modulus (N/nm2)	0.0625	calculated, eq. 1
Microtubule's Cross-Sectional Area (nm2)	337	[14]
Tau Protein's Cross-Sectional Area (nm2)	2.83E-05	estimate
Microtubule's Axial Spring Constant (N/m)	47.1	[14]
Tau Cross-link Axial Spring Constant (N/m)	3.925E-02	[14]

$$k_s = \frac{EA}{l_0} \tag{1}$$

2.4. Boundary Condition and Loadings

The first step of analysis in current project was to validate the proposed model with the work of Peter et al. to make it ready to undergo torsional loading. To obtain results similar to that of Peter et al., the bundle was constraint at one end in all directions and the tensile load was applied at the other end as uniaxial stresses with different magnitude ranging from 1kPa to 10MPa as shown in figure 2.

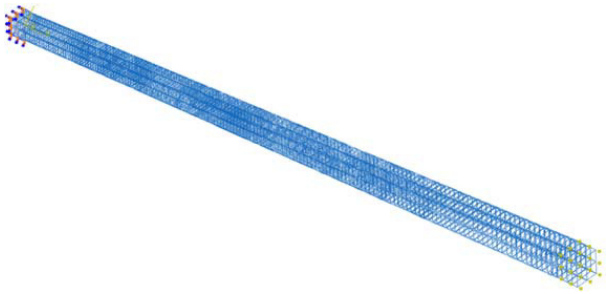

Figure 2. Axonal microtubule bundle constrained at one end and under uniaxial stress on the other end.

These values then converted to force using microtubule's cross-sectional area and applied to each microtubule accordingly. These values are provided in Table 2.

Table 2. Equivalent Forces used in simulations.

Uniaxial Stresses			Equivalent Forces (N)
1kPa	1.00E-15		3.37E-13
10kPa	1.00E-14		3.37E-12
100kPa	1.00E-13	N/nm2	3.37E-11
1MPa	1.00E-12		3.37E-10
10MPa	1.00E-11		3.37E-09

Assuming to have large deformations in this structure, the response of the bundle to tensile loading seems to be nonlinear, although the material properties were all assumed to be linearly elastic.

After validation of the model with the work of Peter et al., we then apply torsional loading on the bundle, as shown in the figure 3, to calculate each bundle's module of rigidity.

Figure 3. Axonal microtubule bundle constrained at one end and torsion on the other end.

The amount of force applied in this step is derived from different trials on each bundle, as to our knowledge, no explicit data are available regarding torsional load applied to axonal bundle in vivo. Surprisingly all the bundles failed at the torsional force equal to 10^{-8}N.nm. So we tested our proposed model with the torsional forces between 10^{-12} to 10^{-9}N.nm and recorded angle of rotation in each step.

3. Results and Discussion

3.1. Bundle steady-state stress-strain behavior

Simulations ran 2μs for all four models of 25, 50, 75, and 100 nanometers cross-sectional spacing with the loads applied following ramp behavior and the following results acquired, Fig. 4-7. In these simulations we assumed that the bundle is under static loading and the results compared for each geometry with that of Peter et al.

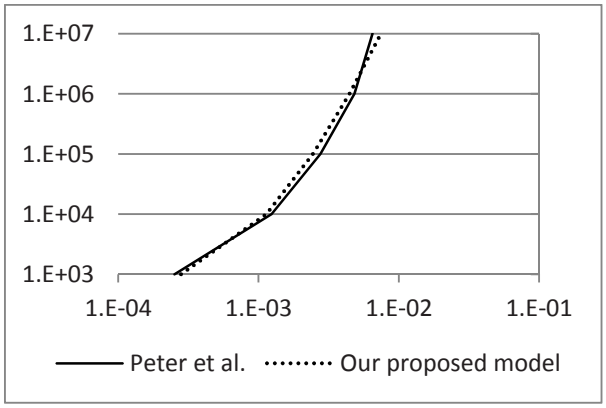

Figure 4. The stress-strain diagram of 100nm cross-sectional spacing bundle compared to that of Peter et al.

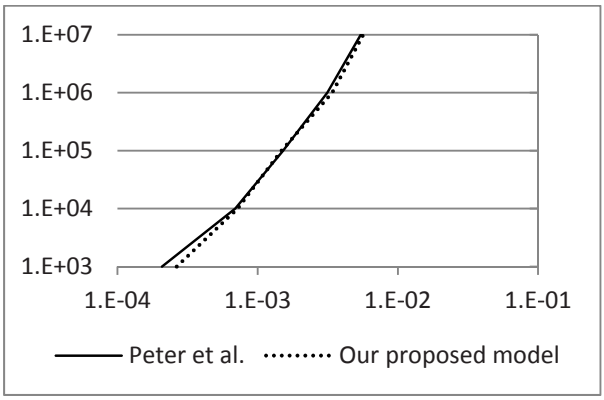

Figure 5. The stress-strain diagram of 75nm cross-sectional spacing bundle compared to that of Peter et al.

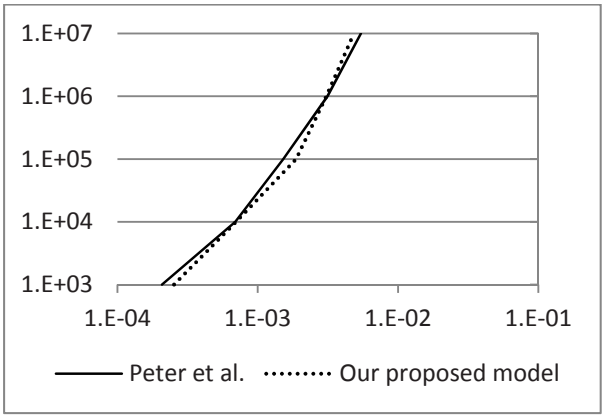

Figure 6. The stress-strain diagram of 50nm cross-sectional spacing bundle compared to that of Peter et al.

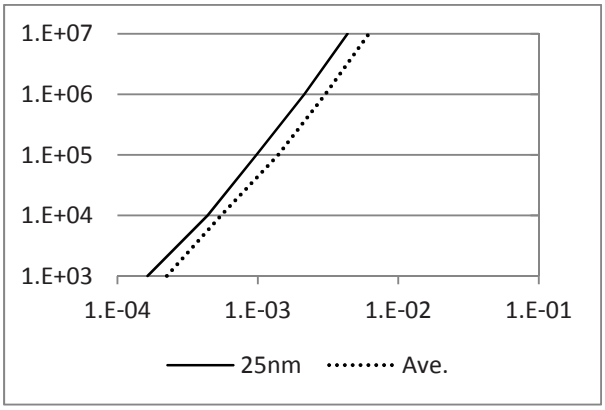

Figure 7. The stress-strain diagram of 25nm cross-sectional spacing bundle compared to that of Peter et al.

The above results are also shown in the table 3 and the t-test has done to compare them. Note must be taken that what is import in comparing the result is total behaviour of the axonal bundles which in both cases clearly show strain-stiffening behaviour of the bundles. Having the power-law fit of the densest cross-link distribution, 25nm average spacing, with the R^2=0.9969, comparing to R^2=0.9963 from the work of Peter et al., gives the confidence

that both bundles are having the same strain-stiffening behaviour.

Table 3. The result of our proposed model under uniaxial loading compared to that of Peter et al.

		Strain in each bundle			
	Stress	100nm	75nm	50nm	25nm
Peter et al.	1kPa	2.52E-04	2.31E-04	2.08E-04	1.64E-04
	10kPa	1.24E-03	9.87E-04	6.92E-04	4.39E-04
	100kPa	2.76E-03	2.17E-03	1.52E-03	9.76E-04
	1MPa	4.83E-03	4.11E-03	3.14E-03	2.14E-03
	10MPa	6.50E-03	5.99E-03	5.44E-03	4.35E-03
Our Proposed Model	1kPa	2.80E-04	2.65E-04	2.54E-04	2.25E-04
	10kPa	1.14E-03	7.20E-04	7.00E-04	5.48E-04
	100kPa	2.44E-03	1.48E-03	1.88E-03	1.40E-03
	1MPa	4.46E-03	3.40E-03	3.09E-03	3.02E-03
	10MPa	7.45E-03	5.66E-03	4.84E-03	6.17E-03
t-test		0.983	0.794	0.971	0.633

Having the same strain-stiffening behaviour of the bundle makes it possible to take the next step to apply torsional loading on the bundles and calculate each bundle module of rigidity, G. Modulus of rigidity is an important factor when the bundle undergoes shear stresses which may happen when, e.g. a bio-engineered scaffold of neural tissue, interacts with the surrounding growing cells.

Table 4 shows each bundle's rotation resulted from application of different torsional loadings.

Table 4. The result of our proposed model under torion.

	θ (deg)			
T (N.nm)	100nm	75nm	50nm	25nm
1.00E-12	1.12E-03	9.78E-04	8.02E-04	5.27E-04
1.00E-11	1.12E-02	9.78E-03	8.02E-03	5.27E-03
1.00E-10	1.12E-01	9.77E-02	8.01E-02	5.27E-02
1.00E-09	1.03E+00	9.11E-01	7.50E-01	4.87E-01

We know that in linear region, when plotting the T- θ diagram, the slope of diagram shows the value of GJ/l according to equation 2.

$$T = \frac{GJ}{l_0}\theta \tag{2}$$

So we have to calculate the value of polar moment of inertia, J, of the bundles. Having the same cross-section, as shown in figure 8, the value of J is equal to 33406642.751nm^4.

Figure 8. Bundle cross-section used to calculate polar moment of inertia.

The T- θ diagram of these bundles is shown in the figure 9. Deriving equation of trend line of each diagram gives the value of GJ/l which is shown in the table 5, with corresponding value of G for each bundle.

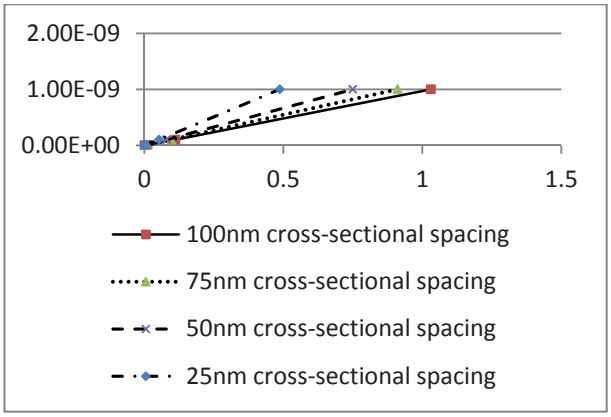

Figure 9. The T- θ curves of bundle in torsion. Curves are shown for 100nm (solid line), 75nm (dotted line), 50nm (dashed line), and 25nm (dash dotted line) cross-link spacing.

Table 5. Calculated values of Modulus of Rigidity, G, for each Cross-link spacing.

Cross-link spacing	100nm	75nm	50nm	25nm
GJ/l (N.nm)	9.7256E-10	1.09986E-09	1.3364E-09	2.05747E-09
G (GPa)	0.233	0.263	0.320	0.493

These results suggest that by increasing the cross-link density in the axonal microtubule bundle, the modulus rigidity increases accordingly. Thus, bundles with the denser cross-link spacing can undergo greater shear stresses without losing their spatial integrity, as they also could bear more tensile stresses.

4. Limitations of the Model

The current model has many assumptions to minimize the computational expenses. We assumed that both microtubule and cross-linking tau proteins follow a linear elastic constitutive relationship which is less valid in compression loadings. We did not include the thermal effects and Brownian motion in the system. The interaction of microtubules with surrounding neurofilaments and the actin cortex did not consider. The effect of polymerization and depolymerization of microtubules resulted from secondary phase of TBI were neglected. Finally, the material parameters of microtubules were based on the current experimental data and as for the tau proteins some assumption made to precede the analysis.

The cross-link tau proteins assumed to be evenly distributed throughout the bundles and the geometry of these proteins estimated as there is no experimental data available by date.

5. Conclusion

The mechanical events which occur at the axons undergo traumatic loading are sophisticated and hard to assess experimentally. This study, to our knowledge, proposed the first 3D finite element model of axonal microtubule bundle under uniaxial tension and torsion.

The bundles showed strain-stiffening behavior under steady state static loading due to distribution of cross-links between microtubules. Validating the proposed model with the work of Peter et al., we could take one step forward to derive the value of modulus of rigidity, G, of each cross-link spacing bundle and shed light to some untouched length scale of axons.

The derived material property, G, of these bundles can be used to select material best collate with the surrounding cells in neural tissue scaffolds which exert both tensional and shear stresses on the scaffold.

With further developing the model to better capture the real behavior of axonal microtubule bundle and combination with biochemical studies of normal and traumatic loading, we would be able to have the better understanding of such complex phenomena as TBI and investigate the possible way to build neural tissue scaffolds and take one step forward in tissue engineering.

Acknowledgments

The authors thank Ms. Sara Makvandi from Islamic Azad University, Science and Research Branch, Department of Biomedical Engineering, for her assistance throughout the project and her helpful discussions and support.

References

[1] Goldstein, L. S. B., and Z. H. Yang. 2000. Microtubule-based transport systems in neurons: the roles of kinesins and dyneins. Annu. Rev. Neurosci. 23:39–71.

[2] Guzik, B.W., and L. S. Goldstein. 2004. Microtubule-dependent transport in neurons: steps towards an understanding of regulation, function and dysfunction. Curr. Opin. Cell Biol. 16:443–450.

[3] Fadic, R., J. Vergara, and J. Alvarez. 1985. Microtubules and caliber of central and peripheral processes of sensory axons. J. Comp. Neurol. 236:258–264.

[4] Yu, W. Q., and P. W. Baas. 1994. Changes in microtubule number and length during axon differentiation. J. Neurosci. 14:2818–2829.

[5] Conde, C., and A. Ca´ceres. 2009. Microtubule assembly, organization and dynamics in axons and dendrites. Nat. Rev. Neurosci. 10:319–332.

[6] Coleman, M. 2005. Axon degeneration mechanisms: commonality amid diversity. Nat. Rev. Neurosci. 6:889–898.

[7] Becker, J. S., and M. Przybylski. 2007. Studies of structure and phosphorylation of tau protein using high resolution mass spectrometry. J. Anal. At. Spectrom. 22:761–765.

[8] Mandelkow, E., Y. H. Song,., E. M. Mandelkow. 1995. On the structure of microtubules, tau, and paired helical filaments. Neurobiol. Aging. 16:347–354.

[9] Ommaya AK, Gennarelli TA. Cerebral concussion and traumatic unconsciousness. Correlation of experimental and clinical observations of blunt head injuries. Brain. 1974; 97(4):633–54.

[10] Gennarelli TA. Mechanisms and pathophysiology of cerebral concussion. J Head Trauma Rehabil. 1986;1(2):23–29.

[11] Alexander MP. Mild traumatic brain injury: Pathophysiology, natural history, and clinical management. Neurology. 1995;45(7):1253–60.

[12] Chandran, P. L., and M. R. K. Mofrad. 2009. Rods-on-string idealization captures semiflexible filament dynamics. Phys. Rev. E. 79:011906.

[13] Mofrad, M. R. K. 2009. Rheology of the cytoskeleton. Annu. Rev. Fluid Mech. 41:433–453.

[14] Stephen J. Peter, Mohammad R.K. Mofrad, Computational Modeling of Axonal Microtubule Bundles under Tension, Biophysical Journal, Volume 102, Issue 4, 22 February 2012, Pages 749-757, ISSN 0006-3495, 10.1016/j.bpj.2011.11.4024.

[15] Klaus-Jurgen Bathe, 1996. “Finite Element Procedures”, Prentice Hall.

[16] Simulia, Abaqus 6.10 (2010).

[17] Kaazempur-Mofrad, M. R., Kamm, Roger (2006). “Cytoskeletal Mechanics: Models and Measurements”, Cambridge University Press.